Chao Liu, Yueqiang Liu, Yue Liu, Guangzhou Hao, Li Li, and Zhirui Wang

Effects of plasma shear flow on the RWM stability in ITER

Effects of plasma shear flow on the RWM stability in ITER

Chao Liu[1], Yueqiang Liu[2,3], Yue Liu[1], Guangzhou Hao[3], Li Li[4], ZhiruiWang[5]

[a]CCFE, Culham Science Centre, Abingdon, Oxon OX14 3DB, UK
[b]Department of Engineering, Cambridge University, UK

Effects of plasma shear flow on the RWM stability in ITER

Chao Liu[1], Yueqiang Liu[2,3,*], Yue Liu[1,*], Guangzhou Hao[3], Li Li[4], Zhirui Wang[5]

[1]Key laboratory of Materials Modification by Laser, Ion and Electron Beams, Dalian University of Technology, Ministry of Education, Dalian 116024, China

[2]CCFE, Culham Science Centre, Abingdon OX14 3DB, United Kingdom

[3]Southwestern Institute of Physics, PO Box 432, Chengdu 610041, China

[4]College of Science, Donghua University, Shanghai 201620, China
[5]Princeton Plasma Physics Laboratory, Princeton, New Jersey 08543, USA

*E-mails of the corresponding authors: Yueqiang.Liu@ccfe.ac.uk; liuyue@dlut.edu.cn

Abstract

Rotational stabilization of the resistive wall mode (RWM), with varying ExB flow shear and the radial location of peak shear, is systematically investigated using the MARS-K code [Liu et al., Phys. Plasmas **15**, 112503 (2008)], following a non-perturbative magnetohydrodynamic-kinetic hybrid approach. The equilibrium is based on a 9MA steady state target plasma from the ITER design, except for the plasma flow profile, which is significantly varied in this study. Generally two branches of unstable $n=1$ kinetic RWMs are computed (n is the toroidal mode number), depending on the flow amplitude. The first unstable branch, which is normally the more unstable one, is sensitively affected by both the local flow shear as well as the radial location of the peak amplitude of the shear. On the contrary, the second unstable branch, which is often weakly unstable, is less affected by the flow shear. Consequently, stability domains are computational mapped out in relevant two-dimensional parameter spaces.

1. Introduction

It is now well understood that stabilization of the resistive wall mode (RWM) is the key solution for increasing the fusion power production in advanced tokamak operations [1]. Provided that the RWM is stable, or is stabilized by certain means, the plasma can in principle overcome the so called Troyon no-wall beta limit [2], and reach the ideal-wall

beta limit, which can be significantly higher. For example, for an ITER plasma studied in Ref. [3], the permissible stable β (where $\beta = 2\mu_0 p_0 / B_0^2$ is the ratio of the plasma pressure, p_0, to the magnetic pressure, and B_0 is the vacuum toroidal magnetic field at the magnetic axis) can be increased by about 40% with stable RWM, resulting in doubling of the fusion power production.

So far, both active control techniques [4-17] using magnetic coils, and passive means, e.g. relying on plasma flow[18-22] and/or kinetic resonance effects from thermal and energetic particles[23-33], have been proposed and experimentally investigated as two effective ways for suppressing the RWM. Whilst active control may have to be the ultimate solution for guaranteeing robust stability of the RWM in ITER, it does require additional hardware components and additional power supplies. More critically, it is certainly not easy, may not even be practical, to install an active control coil system in the future fusion reactor environment. Therefore, it is very desirable if the RWM can be made robustly stable by employing passive control, for instance, by varying the plasma flow and flow shear in a controllable manner. This is the purpose of the present study.

Passive stabilization of the RWM depends on the release, or, damping, of the free energy associated with the mode, via various channels. The primary energy dissipation occurs in the resistive wall, converting a fast growing ideal kink mode into a slowly growing RWM. It is well known that this primary damping mechanism does not change the stability margin of the mode. Further energy damping, which may change the stability margin, has to come from inside the plasma. Several possible free energy-releasing channels inside the plasma have been identified, including the sound wave continuum damping [18,20], the Alfven continuum damping [21,22], the drift kinetic damping due to the mode resonance with particles [23-33], as well as the kinetic damping coupled to additional energy dissipation through resistive layers near rational surfaces [34].

In this work, we consider drift kinetic damping physics for the RWM. We vary the toroidal ExB flow shear of the plasma, which in turn affects the kinetic effects, and thus investigate how the flow shear changes the RWM stability. Within the single fluid theory, the plasma flow is represented by the bulk ion flow, which is the superposition of the ExB flow and the ion diamagnetic flow, with the latter varying roughly linearly with the plasma equilibrium pressure. We choose an ITER equilibrium from the 9MA steady state

scenario, but the flow profile understandably does not follow that predicted for ITER, as that shown in Refs. [10, 26]. We motivate our choice of the flow profiles by two factors. One is the uncertainty associated with the prediction of the ITER plasma rotation (both amplitude and the radial profile). The other is the possibility of actively controlling the flow profile by changing, for example, the neutral beam injection angle or the radial deposition of the ion cyclotron wave heating (which may induce toroidal flow due to mode conversion). In this work, we consider only an ideal plasma model. Only precessional drift resonances of thermal ions and electrons are included, assuming that the achievable toroidal ExB flow is relatively slow in ITER.

We mention that the effect of flow shear on the RWM has been briefly studied in an early work [18], where a fixed shear is assumed. Also only a fluid model was assumed there. Another interesting fluid work reports Kelvin–Helmholtz type of flow shear destabilization of ideal external kink mode, which occurs at flow speed of a significant fraction of the Alfven speed [35]. A semi-analytic result was recently reported showing the flow shear stabilization of the RWM, by choosing a flow regime such that the Landau damping resonance effect is excluded from the consideration [36]. Here we perform a systematic study of the flow shear effect within a kinetic model for the RWM, where the precessional drift resonance plays the key role.

We compute the n=1 RWM stability using the MARS-K code and following a non-perturbative approach [24]. Even though we do not include the finite drift orbit width effects, our results are accurate up to the first order correction in terms of the finite banana width, which holds for precessional drift resonance as established in Ref. [37]. Our key finding is that the toroidal flow shear, as well as the radial location of the peak shear, plays a significant role in the stability of the kinetic RWM.

The following Section briefly describes the toroidal equilibrium that we use. The shear flow is also specified here. Section 3 reports the numerical results, followed by a concluding Section.

2. **Equilibrium specifications**

2.1. Equilibrium for an ITER 9MA steady state plasma

Consider an ITER equilibrium designed for the 9MA steady state scenario, with q_{min}~1.5.

The major radius is R_0=6.2m, with the on-axis vacuum toroidal field of B_0=5.3Tesla. The plasma cross section, as well as the double wall shape, is shown in Fig. 1(a). A slightly simplified wall shape, compared to the actual design, is adopted in this study. A 2D complete wall, with thin-wall approximation, is assumed, with the wall penetration time of about 0.3s for the double wall structure representing the ITER vacuum vessel. This corresponds to the slowest eddy current decay time with the n=1 current pattern.
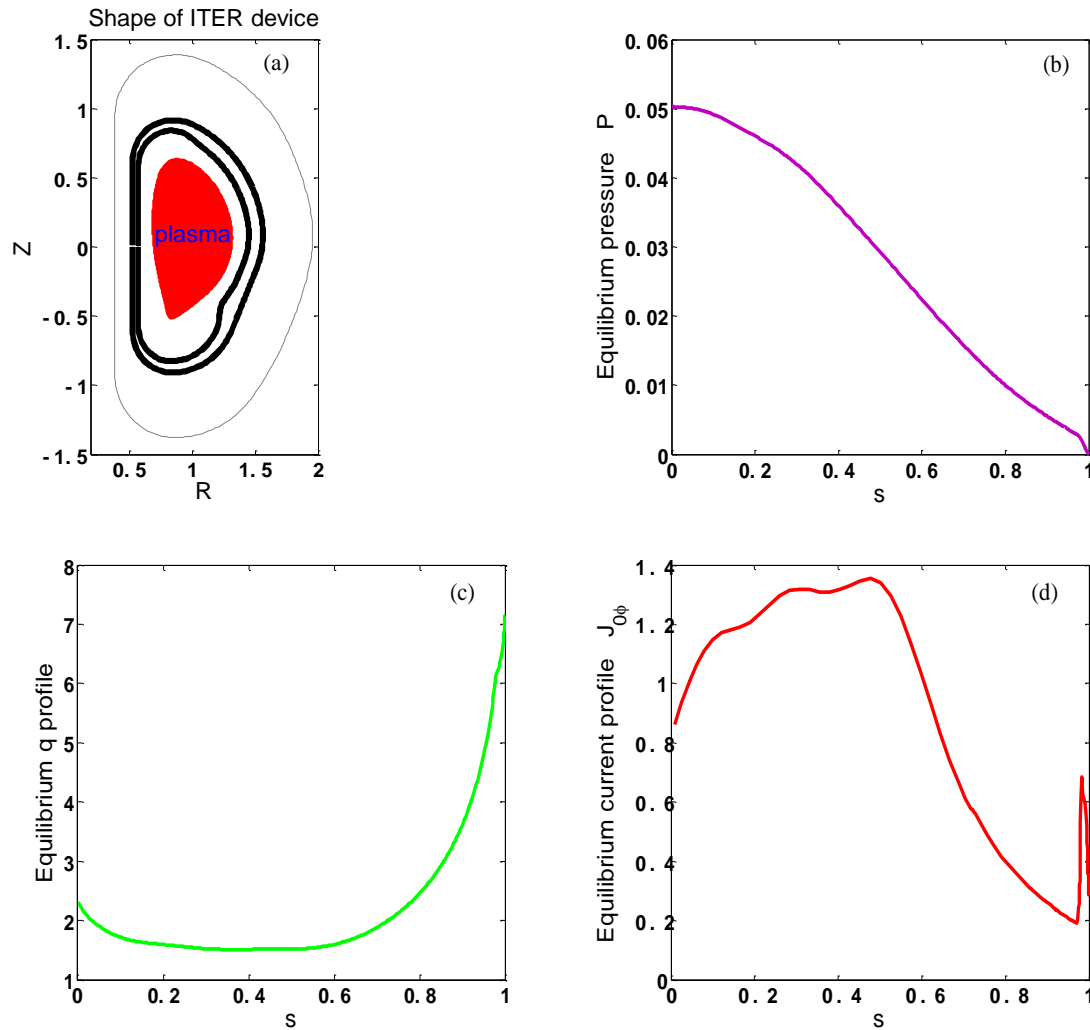

Fig.1. (a) The shape of the equilibrium cross section for the ITER 9MA steady state plasma chosen in this work, plotted together with the simplified shapes of the double-wall vacuum vessel. Note that the (R, Z)-coordinates are normalized by R0 in the plot. Also shown are the radial profiles of the equilibrium quantities for (b) the normalized pressure for the ITER target plasma, (c) the safety factor q, and (d) the normalized surface

averaged toroidal current density. The plasma minor radius is labelled by the normalized equilibrium poloidal flux ψ and $s=\psi^{1/2}$.

Fig.1. (b-d) plot the radial profiles of the target equilibrium pressure, safety factor q, and the surface averaged toroidal current density, respectively. The plasma pressure is normalized by the factor B_0^2/μ_0. The current density is normalized by $B_0/(R_0\mu_0)$. The equilibrium bootstrap current is taken into account in constructing the current profile, resulting in a slightly abnormal variation of the q-profile near the plasma edge.

Shown in Fig.1 is the ITER target equilibrium [27,30,38,39], with the normalized beta $\beta_N=\beta(\%)a(\mathrm{m})B_0(\mathrm{T})/I_p(\mathrm{MA})=2.93$, where β is the plasma volume averaged pressure normalized by the magnetic pressure, and I_p the total plasma current. For the purpose of parametric investigation, we also vary the plasma pressure while fixing the edge q value at $q_a=7.138$, the same as for the target plasma equilibrium. [The target plasma is in divertor configuration. In MARS-K computations, the plasma boundary is slightly smoothed near the X-point, resulting effectively in a limiter configuration for the equilibrium.] This essentially keeps the total plasma current unchanged while varying β_N. This way, we compute the Troyon no-wall beta limit, for the $n=1$ ideal external kink instability, to be $\beta_N^{nw}=2.54$ for this ITER plasma, and the ideal-wall (with the ITER inner wall) beta limit is $\beta_N^{iw}=3.54$. As commonly adopted for the RWM study, we define a linear scaling factor $C_\beta=(\beta_N-\beta_N^{nw})/(\beta_N^{iw}-\beta_N^{nw})$.

2.2. Specification of toroidal ExB flow and flow shear

For the purpose of systematic scans, we choose an analytic specification of the radial profile for the toroidal ExB rotation frequency Ω, with the following model.

$$\Omega(\psi) = \begin{cases} -0.1\psi + c_1 & ;\left[0 \le \psi \le a\right] \\ -0.1\psi - S_\Omega\left(\frac{1}{2}\psi^2 - a\psi\right) + c_2 & ;\left[a < \psi \le \psi_0\right] \\ -0.1\psi - S_\Omega\left(b\psi - \frac{1}{2}\psi^2\right) + c_3 & ;\left[\psi_0 < \psi \le b\right] \\ -0.1\psi + c_4 & ;\left[b < \psi \le 1\right] \end{cases}$$

$c_4 = 0.1$

$c_3 = \frac{1}{2}S_\Omega b^2 + c_4$

$c_2 = S_\Omega \psi_0^2 - S_\Omega(a+b)\psi_0 + c_3$

$c_1 = \frac{1}{2}S_\Omega a^2 + c_2$

$\psi_0 - \delta = a$

$\psi_0 + \delta = b$

Here ψ is the normalized equilibrium poloidal flux labeling the plasma minor radius, with $\psi = 0$ denoting the magnetic axis, and $\psi = 1$ corresponding to the plasma boundary surface. The above model allows, on top of a global rotation profile, a local variation of the rotation shear near $\psi = \psi_0$ (ψ_0 corresponds to the radial location of the peak value of the rotation shear amplitude). The local flow shear is determined by the parameter S_Ω in the model, which does not follow the exact shear definition, but is closely related to the shear via the following expression

$$S_\Omega = \frac{\left[d\Omega/d\psi\right]_{\psi=b} - \left[d\Omega/d\psi\right]_{\psi=\psi_0}}{\delta}.$$

We shall call S_Ω the normalized flow shear parameter, which is a good indicator of the local flow shear. The parameter δ defines the radial extent of the local shear variation. In further numerical study, we fix $\delta = 0.1$. We point out that the above specification only defines the rotation profile. The rotation amplitude is varied by introducing the on-axis rotation frequency Ω_0. While scanning Ω_0, the entire plasma rotation profile is scaled. Finally, we also introduce quantities $s = \sqrt{\psi}$, $s_0 = \sqrt{\psi_0}$. In further study, we shall exploit the RWM stability in the parameter space specified by s_0, S_Ω, Ω_0, and C_β.

For the drift kinetic resonance effects considered in this work, the crucial role is

played by the matching between the ExB flow frequency and the precessional drift frequency of thermal ions and electrons. Figure 2 shows three ExB flow profiles, constructed according to the above flow model with $\Omega_0=0.02\Omega_A$ ($\Omega_A=R_0\,(\mu_0\rho_0)^{1/2}/B_0$ is the on-axis Alfven frequency, with ρ_0 being the plasma core density), $S_\Omega=9$, and $s_0=0.35,0.55,0.75$, respectively, together with the thermal ion precessional drift frequency $\langle\Omega^i_d\rangle$, averaged over the particle (Maxwellian) equilibrium distribution as well as over the magnetic surface, for the ITER target plasma. The electron toroidal precession has a reversed sign compared to the ion precession. For comparison, we also plot the ion diamagnetic rotation frequency Ω_{*i} for this ITER plasma.
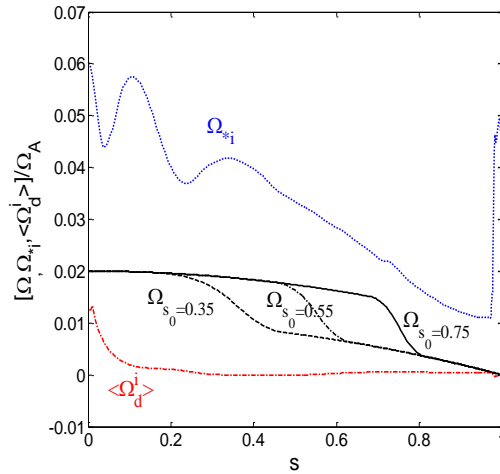

Fig.2. Three examples of the ExB *flow profiles with a large local shear ($S_\Omega=9$, $\Omega_0=0.02\Omega_A$) located at $s_0=0.35,0.55,0.75$, respectively, plotted together with the thermal ion precessional drift frequency, averaged over the particle phase space (energy and pitch angle) equilibrium distribution and along the magnetic flux surface, and with the thermal ion diamagnetic frequency for the target plasma. All frequencies are normalized by the on-axis Alfven frequency Ω_A.*

Figure 2 shows that a proper resonance condition, between the ExB flow and the averaged toroidal precession, is satisfied only at slow plasma rotation. This is indeed confirmed by further MARS-K computations shown in Section 3.

3. Numerical results and discussions

The computational results presented below are obtained by the MARS-K code [24], following a non-perturbative MHD-kinetic hybrid approach. In this approach, the single fluid MHD equations, linearized around a given equilibrium, are solved with a drift kinetic closure replacing the standard adiabatic ideal gas assumption. This involves two key changes to the standard MHD model. First, the perturbed plasma pressure is kinetically evaluated by solving the perturbed drift kinetic equation for plasma particles, resulting in an anisotropic perturbed pressure (pressure tensor), which replaces the scalar, isotropic perturbed pressure for the equation of state in the standard fluid formulation. Secondly, in the momentum equation, the force term associated with the perturbed pressure gradient is now replaced by the divergence of the perturbed pressure tensor.

The resulting coupled MHD-kinetic equations are solved as a generalized eigenvalue problem, where the real and imaginary parts of the (generally) complex eigenvalue represent the growth rate and real frequency of the RWM, respectively. Because the eigenvalue also enters, in a strongly non-linear form, into drift kinetic integrals via the resonance operator, this opens the possibility of existence of multiple unstable branches for the same RWM [40, 41], which is often referred to as the kinetic RWM in this work. For comparison, we shall also compute the eigenvalue of the mode under fluid approximation, where the drift fluid closure is replaced by the standard equation of state for ideal gas. The resulting RWM is referred to as the fluid RWM. Finally, we mention that in this work, the fluid flow is also included into the MHD part of the equation via inertial forces as in Ref. [33], under the assumption of subsonic flow.

Detailed description of the MARS-K formulation is reported in Ref. [24], with systematic code benchmarking efforts presented in Ref. [39].

3.1. Generic characteristics of the non-perturbative kinetic solution

For this ITER equilibrium, and with the chosen flow profile, the MARS-K non-perturbative computations typically find two unstable branches for the $n=1$ kinetic RWM. Figures 3 and 4 show two examples at $C_\beta=90\%$ and 70%, respectively. We choose the flow profile with $s_0=0.75$ and $S_\Omega=9$, and scan the rotation amplitude Ω_0. The toroidal

precessional drift resonance of thermal ions and electrons are taken into account in the kinetic module.

Figure 3 (a) and (b) plot the normalized growth rate and the real frequency of the RWM, respectively. The normalization factor is the MARS-K computed slowest $n=1$ eddy current decay time, τ_w, of the double wall structure in vacuum. At $C_\beta=90\%$, the two unstable branches co-exist at a given rotation speed. The first branch, which is more unstable at fast flow, has a large real frequency compared to the second branch. On the other hand, the frequency range of the first branch solution is still comparable to the mode growth rate, which is relatively high since the plasma pressure is close to the ideal wall beta limit. What is unusual for this high beta case is that the two branches have comparable growth rates at slower rotation frequency around $0.01\Omega_A$. With further decreasing of the flow speed, the second branch becomes predominantly unstable. Overall, due to the overlap of two unstable branches, no stability window exists for this high beta equilibrium, with varying plasma flow speed.

We point out that, at very high beta (when beta is approaching the ideal-wall beta limit), the thin shell model adopted in MARS-K may not be sufficiently accurate. This is because the magnitude of the mode eigenvalue becomes large, resulting in a thin skin depth in the wall. When the skin depth is much smaller than the wall thickness, we expect a substantial modification of the RWM stability by a thick wall [42]. For the results shown in Fig. 3, the first unstable branch has eigenvalue amplitude (normalized by the wall time) varying between 20 and 50. We estimate the skin depth due to this instability to be about 0.07m to 0.12m for the ITER wall. This range is slightly above the thickness of the vacuum vessel, which is 0.06m. We expect a slight modification of the numerical results presented here for the first branch, if the finite wall thickness effect were taken into account. For the second branch, the amplitude of the eigenvalue is still small. The thin wall approximation should be accurate.
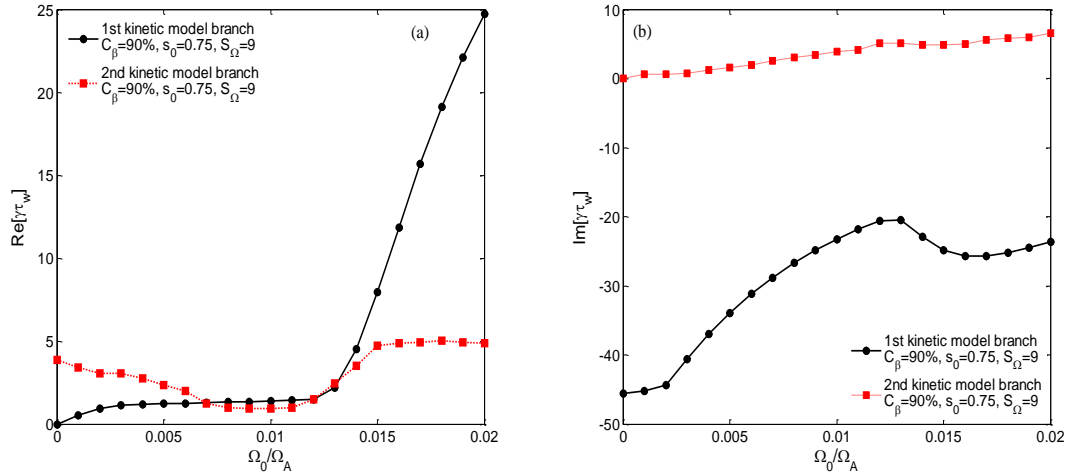
Fig.3. The (a) real, and (b) imaginary, parts of the computed eigenvalue of the kinetic RWM, versus the on-axis ExB rotation frequency Ω_0. The eigenvalue is normalized by the slowest n=1 double wall eddy current decay time τ_w in vacuum. An equilibrium with $C_\beta=90\%$, and a shear flow with $s_0=0.75$ and $S_\Omega=9$ are considered.

The co-existence of two unstable branches occurs only at sufficiently high plasma pressures. At lower plasma pressure, the two-solution structure is somewhat different, as shown by Fig. 4. In this case, the two unstable branches do not co-exist at a given rotation. Instead, at fast flow, $\Omega_0>0.01\Omega_A$, the first branch appears, with relatively large mode frequency; at slow flow, $\Omega_0<0.006\Omega_A$, the second unstable branch appears, with small mode frequency. A stable window emerges between $\Omega_0>0.006\Omega_A$ and $\Omega_0<0.01\Omega_A$, where no unstable RWM is found. As will be shown later on, this stable window also depends on the amplitude and radial location of the flow shear.
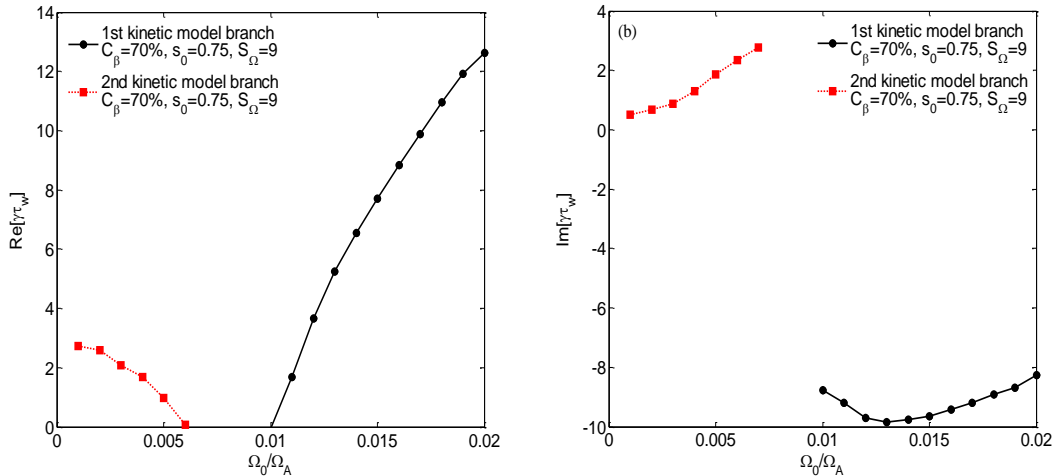
Fig.4. The (a) real, and (b) imaginary, parts of the computed eigenvalue of the kinetic RWM, versus the on-axis ExB *rotation frequency* Ω_0. *The eigenvalue is normalized by the slowest n=1 double wall eddy current decay time* τ_w *in vacuum. An equilibrium with* C_β=70%, *and a shear flow with* s_0=0.75 *and* S_Ω=9 *are considered.*

The two-branch solution is primarily a consequence of the drift kinetic effects. Figure 5 compares the kinetic solution with the fluid solution where the kinetic physics are switched off. Here we scan the plasma pressure factor C_β while fixing the rotation amplitude at Ω_0=0.001Ω_A, as well as the flow shear at s_0=0.75 and S_Ω=9. Figure 5 (a) and (b) plot the growth rate and frequency of the mode, respectively. Note that the growth rate of the first kinetic RWM branch is multiplied by a factor of 10 in Fig. 5(a) for a more clear comparison. This branch appears only at sufficiently high beta. The second branch follows the trend of the fluid solution, for both the growth rate and the mode frequency. This branch can be viewed as the drift kinetic version of the fluid RWM, but is more stable than the fluid version [10, 18, 19]. In fact the marginal stability point, in terms of C_β, also shifts upwards with the inclusion of the drift kinetic damping.

On the other hand, the characteristics of first branch are rather different from that of the fluid solution. This can be viewed as a kinetic-driven branch for the RWM. The mode frequency is higher, though still remains in the RWM frequency range, as shown by Fig. 5(b) (note that the sign-reversed frequency is plotted here for the first branch). More importantly, this branch is much more unstable at faster rotation, as shown in Figs. 3 and 4. It is for this reason; we shall systematically investigate the stability of the first branch in later sub-sections.
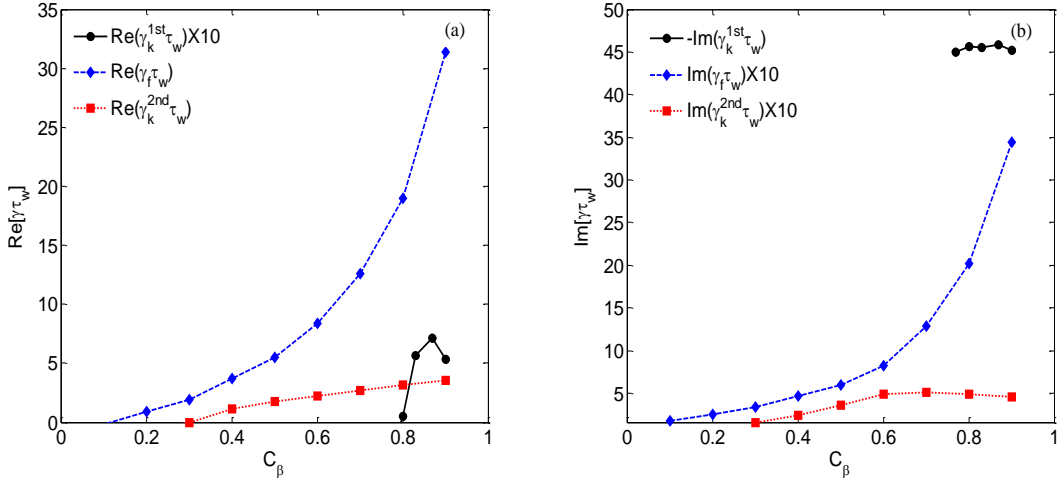
Fig.5. The (a) real, and (b) imaginary, parts of the computed eigenvalue of the RWM versus equilibrium pressure scaling factor C_β. Compared are the eigenvalue γ_f following the single fluid model, and the two-branch solutions γ_k following the non-perturbative fluid-kinetic hybrid model. An ExB flow, with $\Omega_0 = 0.001\Omega_A$, $s_0=0.75$ and $S_\Omega=9$, is considered.

Figure 6 compares the computed RWM eigenmode structure, for selected data points from Figs. 3-5. We plot the dominant poloidal Fourier harmonics (m=0,...,3 in an equal-arc magnetic coordinate system) of the radial displacement. The amplitude of the eigenfunction is in arbitrary units. Compared with the fluid RWM eigenmode structure, the drift kinetic modification is not significant. A slightly larger modification is observed for the second branch at slow rotation.   This seems to indicate that the occurrence of the double branch kinetic solution is mainly associated with the non-linear dependence of the kinetic resonance operators on the RWM eigenvalue [43, 40, 41].
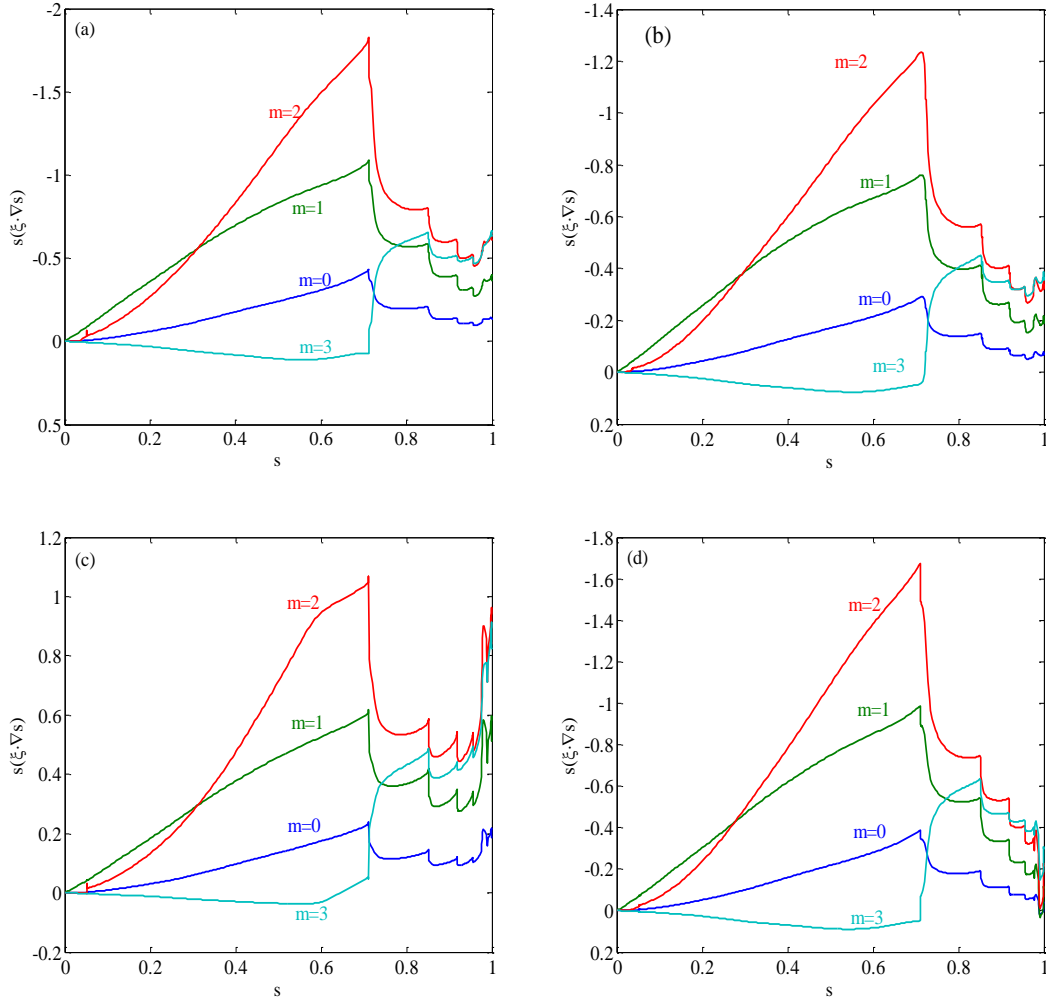
Fig.6. The computed eigenfunctions of the RWM, in terms of the poloidal Fourier harmonics (in an equal-arc magnetic coordinate system) of the plasma radial displacement, for an equilibrium with $C_\beta=90\%$, $s_0=0.75$ and $S_\Omega=9$. Compared are the eigenfunctions of (a) the fluid RWM at $\Omega_0=0.001\Omega_A$, (b) the first branch of the kinetic RWM at $\Omega_0=0.02\Omega_A$, (c) the second branch of the kinetic RWM at $\Omega_0=0.001\Omega_A$, and (d) the second branch of the kinetic RWM at $\Omega_0=0.02\Omega_A$.

3.2. Varying radial location of peak flow shear

In this subsection, we investigate the stability of the kinetic RWM, while varying the radial location of the peak flow shear. We focus on the first branch of the kinetic solution, which generally has much larger growth rate than the second branch. Due to the large dimension of the possible parametric space, we restrict ourselves on one choice of the

rotation shear, namely $S_\Omega=9$. The effect of varying flow shear will be reported in the next subsection.

Figure 7 (a) and (b) plot the mode growth rate as a function of s_0, for the first kinetic branch and for the fluid RWM, respectively, for the high beta case with $C_\beta=90\%$. Three relatively fast rotation frequencies are considered (for which the first branch generally has large growth rates). Several observations can be made from Fig. 7. (i) The flow shear location has rather different effect on the kinetic RWM, than the fluid counterpart. The dependence of the kinetic growth rate on s_0 is in general more complicated than that of the fluid growth rate. (ii) For the kinetic RWM, a narrow stability window can open around $s_0=0.7$, whilst for the fluid model, a more robust stabilization occurs at $s_0>0.7$. (iii) The fact that the kinetic stabilization of the mode occurs near $s_0=0.7$, is directly related to the peak location of the mode eigenfunction as shown in Fig. 6. This implies that, according to the drift kinetic theory, the strongest mode damping is achieved, if a large flow shear can be tuned near the radial location where the displacement associated with the RWM peaks.
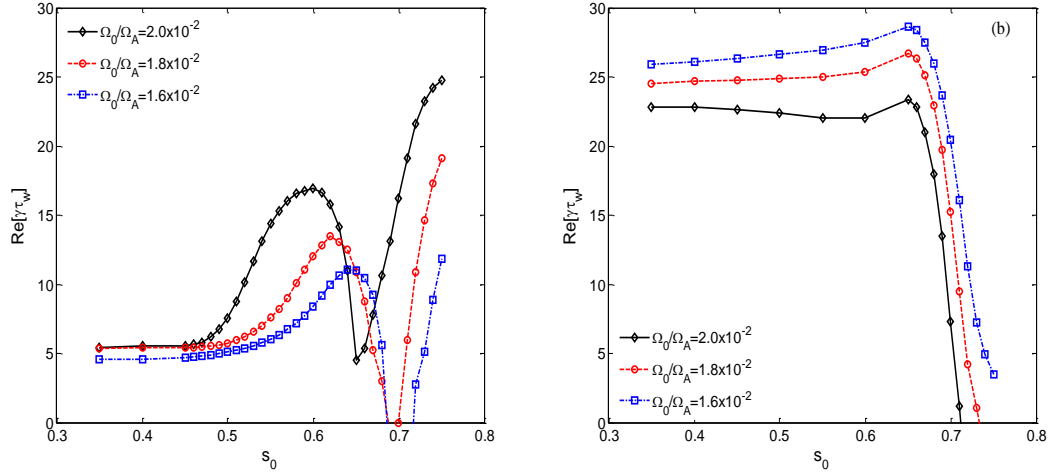

Fig.7. The normalized growth rate of (a) the first branch of the kinetic RWM, and (b) the fluid RWM, versus the radial location s_0 of the flow shear peaking, for three choices of the on-axis ExB rotation frequency $\Omega_0=0.016\Omega_A$, $0.018\Omega_A$, and $0.02\Omega_A$, respectively. An equilibrium with $C_\beta=90\%$ is considered. The normalized flow shear parameter is fixed at

$S_\Omega=9$.

Figure 7(a) also shows that the width of the stability window for the kinetic RWM depends on the rotation amplitude Ω_0. A more comprehensive picture is shown in Fig. 8, where the mode growth rate is plotted in the 2D parameter space (Ω_0, s_0). The stability window opens up at about $\Omega_0=0.018\,\Omega_A$. The width of the window, in s_0, increases with decreasing Ω_0. It is interesting to note that the lower boundary of the stability window, shown in Fig. 8, hardly changes with Ω_0, but the upper boundary quickly expands.
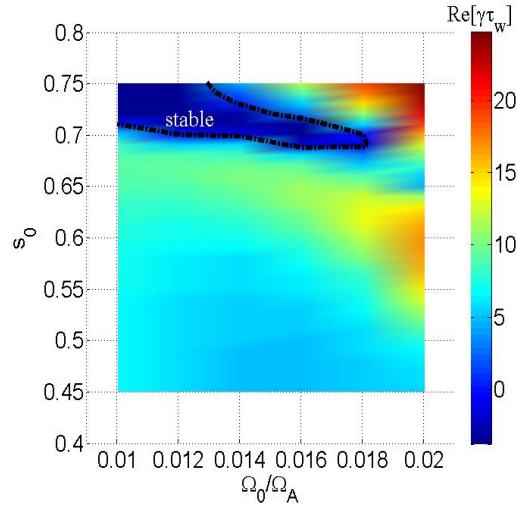
Fig.8. The growth/damping rate for the first branch of the kinetic RWM, plotted in the 2D parameter space (Ω_0, s_0). An equilibrium with $C_\beta=90\%$ is considered. The normalized flow shear parameter is fixed at $S_\Omega=9$. The dash-dotted curve shows the stability margin.

The small stability window presented in Figs.7 (a) and 8 corresponds to the worst-case scenario, which holds at very high beta ($C_\beta=90\%$). The stable window can be significantly wider for equilibria at lower beta. Figure 9 shows one example for $C_\beta=70\%$, compared with the $C_\beta=90\%$ case, at the flow speed of $\Omega_0=0.02\Omega_A$. At $C_\beta=70\%$, the lower boundary of the stable window effectively disappears, resulting in a large stable region in the s_0 space. The upper boundary of the stability window remains, with $s_0=0.65$ for this case.
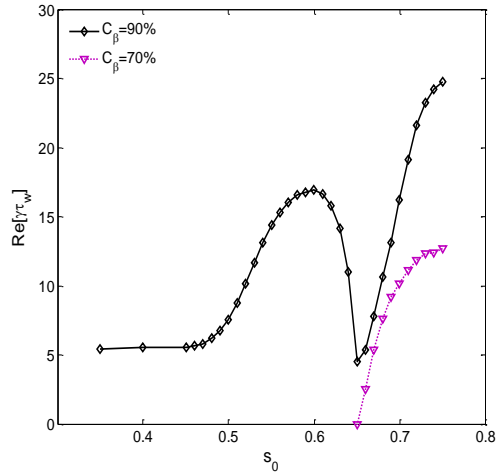
Fig.9. Comparison of the growth rate for the first branch of the kinetic RWM, with varying radial location s_0 of the flow shear peaking, for two choices of the plasma pressure scaling parameter $C_\beta = 70\%$ and $C_\beta = 90\%$, respectively. Fixed are the on-axis ExB rotation frequency $\Omega_0 = 0.02\Omega_A$, and the normalized flow shear parameter $S_\Omega = 9$.

3.3. Varying peak amplitude of flow shear

In the results presented so far, we have fixed the peak amplitude of flow shear, characterized by the normalized shear parameter $S_\Omega = 9$. In what follows, we study the effect of varying S_Ω on the stability of the kinetic RWM. We fix the radial location of the shear peak at $s_0 = 0.75$. Figure 10 shows three rotation profiles, with $S_\Omega = 1, 5, 9$, respectively.
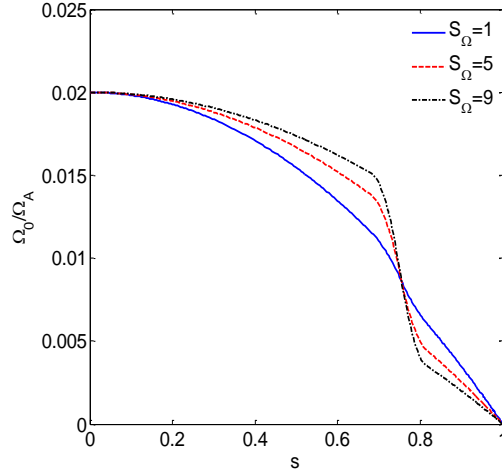
Fig.10. Three examples of the ExB *rotation profiles, with different flow shear at $S_\Omega=1, 5,$ 9, respectively. The radial locations of the flow shear peaking is fixed at $s_0=0.75$.*

Figure 11 compares the growth rate, as a function of the flow amplitude, of the first branch of the kinetic RWM (a), with that of the fluid RWM (b), for the $C_\beta=70\%$ case. We use three rotation profiles as shown in Fig. 10. We first note the qualitative difference of the flow shear effect on the RWM, between the kinetic and the fluid models. With the kinetic model, which offers a better description of the RWM physics by properly including the mode-particle resonances, the flow shear tends to stabilize the mode at fast flow, but slightly destabilize the mode at slower flow speed. The transition from stabilization to destabilization occurs at about $\Omega_0=0.014\Omega_A$ for our case. As a result of destabilization, the marginal stability point, in terms of the rotation amplitude, shifts down with increasing the local flow shear.

The flow and flow shear effect is qualitatively different following the fluid model, as shown in Fig. 11(b). The growth rate of the mode monotonically decreases with increasing the flow speed. The local flow shear has a minor influence on the mode stability. For our case, the fluid theory predicts a full stabilization of the RWM at $\Omega_0>0.025\Omega_A$.
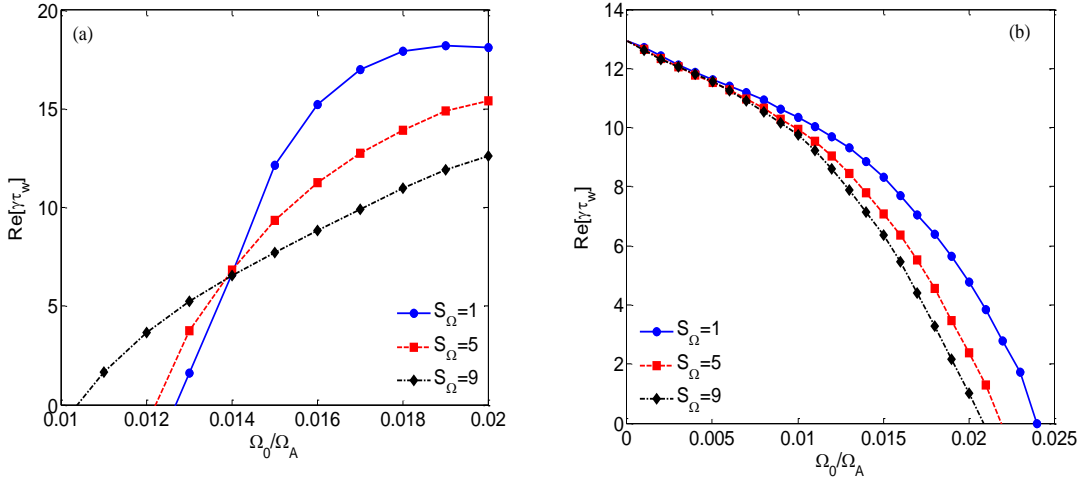
Fig.11. *The normalized growth rate of (a) the first branch of the kinetic RWM, and (b) the fluid RWM, versus the on-axis ExB rotation frequency Ω_0, with varying flow shear at S_Ω=1, 5, 9, respectively. The radial location s_0 of the flow shear peaking is fixed at 0.75. An equilibrium with C_β=70% is considered.*

Figure 12 shows the stability diagram for the first unstable branch of the kinetic RWM, from a more systematic scan of the flow shear. The marginal stability curve, shown by the dash-dotted line, is mapped out in the 2D parameter space (Ω_0, S_Ω). The primary effect here is the full stabilization of the first branch at slow flow speed, resulted from the precessional drift resonance damping. The stable domain slightly shrinks with increasing the flow shear. The other interesting effect is the significant reduction of the RWM growth rate in the unstable domain when $\Omega_0 > 0.013 \Omega_A$, as the flow shear increases.
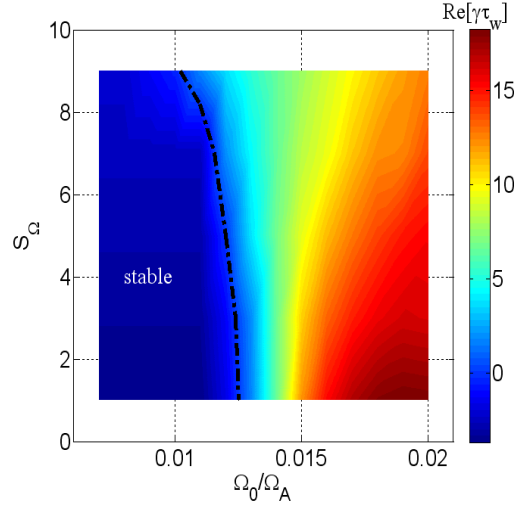
Fig.12. The growth/damping rate for the first branch of the kinetic RWM, plotted in the 2D parameter space (Ω_0, S_Ω). The radial location s_0 of the flow shear peaking is fixed at 0.75. An equilibrium with $C_\beta=70\%$ is considered. The dash-dotted curve shows the stability margin.

The kinetic stabilization shown in Fig. 11(a) and Fig. 12 occurs for the first unstable branch, which is the more unstable one. However, at sufficiently high beta, the second branch is also weakly unstable as shown by Figs. 3 and 4. This second unstable branch is affected by the flow and flow shear as well. As a result, the overall stability of the kinetic RWM is determined by the stability of both unstable branches. This is illustrated in Fig. 13, where we plot the RWM stability diagrams in the 2D parameter space (Ω_0, C_β). Two cases, with the normalized flow shear parameter (a) $S_\Omega=1$, and (b) $S_\Omega=9$, are compared.

A stable domain still exists for the kinetic RWM when both branches are taken into account. The marginal stability curve (thick dash-dotted line) is defined by both branches. In particular, the first branch determines the stability boundary from the right side of the stable domain, whereas the second branch largely determines the stability boundary from the top. At sufficiently slow flow and sufficiently low beta, the RWM is fully stable according to the non-perturbative drift kinetic computations. A larger flow shear slightly expands the upper boundary of the stable domain by stabilizing the second unstable kinetic RWM branch. A larger expansion occurs for the right boundary of the

stable domain, as a result of flow shear stabilization of the first unstable branch. As a final observation, we note that the instability of the second unstable branch is generally very weak. This weak instability may easily be overcome by including additional damping mechanisms that are not considered in this work, for instance, that from trapped energetic particles. This may results in a significant upwards expansion of the stable domain in Fig. 13. On the other hand, the right-wards expansion may be more problematic, due to the strong instability of the first unstable branch.
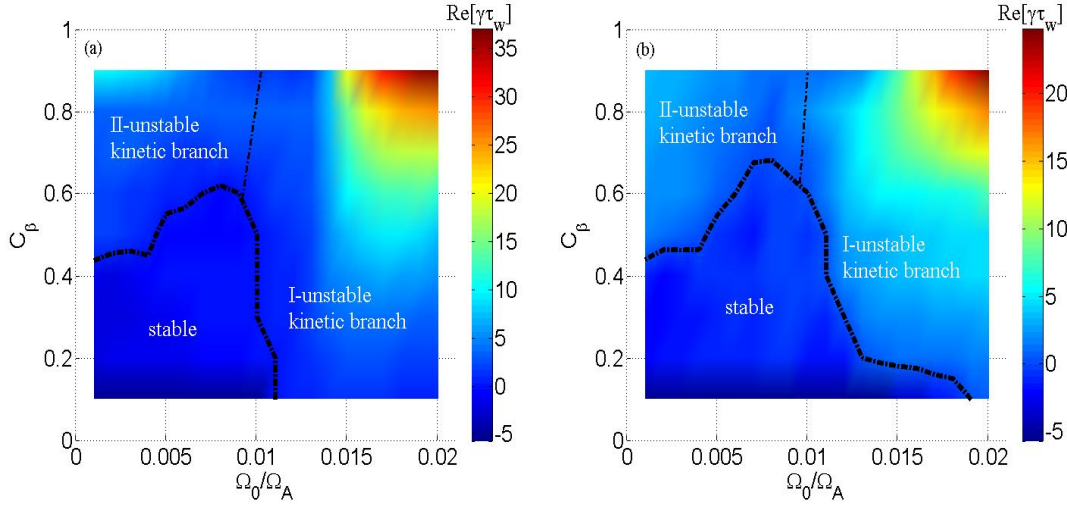

Fig.13. The growth/damping rate for both branches of the kinetic RWM, plotted in the 2D parameter space (Ω_0, C_β), for (a) $S_\Omega=1$, and (b) $S_\Omega=9$. The radial location s_0 of the flow shear peaking is fixed at 0.75. The thick dash-dotted curves show the overall stability margin. The thin dashed-dotted lines show the approximate separation between the two unstable branches.

4. Conclusion

A non-perturbative MHD-kinetic hybrid formulation is applied to computationally study the RWM stability for an ITER 9MA steady state plasma. In particular, we focus on a systematic investigation of the role of the plasma ExB flow shear on the passive stabilization of the mode. This is motivated by the uncertainty in the prediction of the flow profile in ITER, as well as by the desire of actively (locally) controlling the flow shear as a tool for the suppression of the RWM stability.

A general feature of the kinetic prediction is the existence of two unstable branches for this ITER plasma. The first branch has somewhat higher mode frequency, though still remains in the frequency range for the RWM. More importantly, this branch has much higher growth rate compared to the second branch, and hence poses the most severe limitation on the stability window for the mode.

We find that the first unstable branch is sensitively affected by both the local flow shear as well as the radial location of the peak amplitude of the shear. At high beta (C_β=90%), a narrow stable window appears as we vary the radial location of the shear peak. Not surprisingly, the optimal shear location correlates to the peak location of the RWM eigenfunction (in terms of the plasma radial displacement). The stable window significantly expands as we lower the plasma pressure. At a fixed radial location, a large local flow shear strongly reduces the growth rate of the first unstable branch of the kinetic RWM, but meanwhile slightly increases the critical flow amplitude required for complete suppression of the mode.

The second unstable branch is generally only weakly unstable. The flow shear has less dramatic effect on the stability of this branch. However, even taking into account this weak instability, there is still a reasonably wide stable domain for the RWM, in the (Ω_0, C_β) space. A larger flow shear further widens the stable domain, mainly by stabilizing the first unstable branch.

In this work, we have not yet included the drift kinetic effects from trapped energetic particles (EPs), produced either by auxiliary heating or by the fusion reaction itself (i.e. DT born alphas). The EPs normally have much higher precessional drift frequency than thermal particles, and hence can hardly be in resonance with the RWM at slow flow. Despite this, the EPs can still contribute to the kinetic damping of the RWM [29, 30, 34, 44, 45], especially at higher flow speed. One future work is to investigate the role of the flow shear on the RWM, with the inclusion of the kinetic effects from EPs. We also neglected the particle collisions in this study [46]. Whist being a reasonable assumption for thermal ions in ITER, this is an approximation for thermal electrons.

References

[1]Hender T C *et al* Progress in the ITER Physics Basis Chapter 3: MHD stability, operational limits and disruptions 2007 *Nucl. Fusion* **47** S128-S202

[2]Troyon F *et al* 1984 *Plasma Phys. Control. Fusion* **26** 209-215

[3]Liu Y Q *et al* 2009 *Nucl. Fusion* **49** 035004

[4]Liu Y Q *et al* 2000 *Phys. Rev. Lett.* **84** 907

[5]Liu Y Q *et al* 2000 *Phys. Plasmas* **7** 3681

[6]Bialek J *et al* 2001 *Phys. Plasmas* **8** 2170

[7]Chance M S *et al* 2002 *Nucl. Fusion* **42** 295

[8]Chu M S *et al* 2003 *Nucl. Fusion* **43** 441

[9]Chu M S *et al* 2004 *Phys. Plasmas* **11** 2497

[10]Liu Y Q *et al* 2005 *Nucl. Fusion* **45** 1131

[11]Okabayashi M *et al* 2005 *Nucl. Fusion* **45** 1715

[12]Sabbagh S A *et al* 2006 *Phys. Rev. Lett.* **97** 045004

[13]Merkel P *et al Fusion Energy 2006 (Proc. 21st Int. Conf. Chengdu, 2006) (Vienna: IAEA) CD-ROM fileTH/P3-8 URL* http://www-naweb.iaea.org/napc/physics/FEC/FEC2006/html/index.htm

[14]Strumberger E *et al* 2008 *Phys. Plasmas* **15** 056110

[15]Albanese R *et al* 2008 *IEEE Trans. Magn.* **44** 1654

[16]Portone A *et al* 2008 *Plasmas Phys. Control. Fusion* **50** 085004

[17]Liu Y Q 2009 *Plasma Phys. Control. Fusion* **51** 115006

[18]Bondeson A *et al* 1994 *Phys. Rev. Lett.* **72** 2709

[19]Chu M S *et al* 1995 *Phys. Plasmas* **2** 2236

[20]Betti R *et al* 1995 *Phys. Rev. Lett.* **74** 2949

[21]Gregoratto D *et al* 2001 *Plasma Phys. Control. Fusion* **43** 1428-1439

[22]Zheng L J *et al* 2005 *Phys. Rev. Lett.* **95** 25503

[23]Hu B *et al* 2004 *Phys. Rev. Lett.* **93** 105002

[24]Liu Y Q *et al* 2008 *Phys. Plasmas* **15** 092505

[25]Liu Y Q *et al* 2008 *Phys. Plasmas* **15** 112503

[26]Liu Y Q *et al* 2009 *Nucl. Fusion* **49** 035004

[27]Zheng L J *et al* 2010 *Phys. Plasmas* **17** 056104

[28]Berkery J W *et al* 2010 *Phys. Rev. Lett.* **104** 035003

[29]Berkery J W *et al* 2010 *Phys. Plasmas* **17** 082504

[30]Liu Y Q 2010 *Nucl. Fusion* **50** 095008

[31]Hao G Z *et al* 2011 *Phys. Rev. Lett.* **107** 015001

[32]Wang Z R *et al* 2012 *Phys. Plasmas* **19** 072518

[33]Mendard J E *et al* 2014 *Phys. Rev. Lett.* **113** 255002

[34]He Y L *et al* 2014 *Phys. Rev. Lett.* **113** 175001

[35]Chapman I T *et al* 2011 *Plasma Phys. Control. Fusion* **53** 125002

[36]Junya Shiraishi *et al* 2014 *Plasma and Fusion Research* **9** 3403027

[37]Liu Y Q *et al* 2014 *Phys. Plasmas* **21** 056105

[38]Villone Fabio *et al* 2010 *Nucl. Fusion* **50** 125011

[39]Berkery J W *et al* 2014 *Phys. Plasmas* **21** 052505

[40]Liu Y Q *et al* 2009 *Phys. Plasmas* **16** 056113

[41]Berkery J W *et al* 2011 *Phys. Plasmas* **18** 072501

[42]Pustovitov V D 2012 *Phys. Plasmas* **19** 062503

[43]Fitzpatrick R *et al* 1996 *Nucl. Fusion* **36** 11

[44]Chapman I T *et al* 2011 *Plasma Phys. Control. Fusion* **53** 065022

[45]Chapman I T *et al* 2013 *Phys. Plasmas* **20** 056101

[46]Berkery J W *et al* 2011 *Phys. Rev. Lett.* **106** 075004